

Dynamics of the interaction between the rotor and the induction zone

This content has been downloaded from IOPscience. Please scroll down to see the full text.

2016 J. Phys.: Conf. Ser. 753 072024

(<http://iopscience.iop.org/1742-6596/753/7/072024>)

[View the table of contents for this issue](#), or go to the [journal homepage](#) for more

Download details:

IP Address: 130.226.56.2

This content was downloaded on 02/11/2016 at 13:42

Please note that [terms and conditions apply](#).

You may also be interested in:

[Rotor thermal stress monitoring in steam turbines](#)

Boubelík Antonín, Jakl Jan and Liška Jindich

[Quantum to Classical Transition in a System of Two Coupled Kicked Rotors](#)

Zhao Wen-Lei and Jie Quan-Lin

[Stall-Induced Vibrations of the AVATAR Rotor Blade](#)

M Stettner, M J Reijerkerk, A Lünenschloß et al.

[CFD computations of the second round of MEXICO rotor measurements](#)

Niels N. Sørensen, F. Zahle, K. Boorsma et al.

[Simulations of wind turbine rotor with vortex generators](#)

Niels Troldborg, Frederik Zahle and Niels N. Sørensen

[Finding the ideal strategy: Full-scale fatigue testing of wind turbine rotor shafts](#)

T Rauert, J Herrmann, P Dalhoff et al.

[Rotor clearance design and evaluation for an oil injected twin screw compressor](#)

D Buckney, A Kovacevic and N Stosic

Dynamics of the interaction between the rotor and the induction zone

Mahmood Mirzaei, Alexander R. Meyer Forsting and Niels Troldborg

DTU Wind Energy, Technical University of Denmark, Frederiksbergvej 399, 4000 Roskilde, Denmark

E-mail: {mmir, alrf, niet}@dtu.dk

Abstract. Traditionally met masts are used for power and load verifications. They are normally placed 2-4 rotor diameters ahead of the turbine. However in complex terrain this can lead to complex analysis of the effect of the terrain on the flow field. A nacelle mounted lidar can provide a better tool for wind field measurements in all terrains. Provided that the measurement is close enough to the rotor disc, the uncertainty in the flow field measurement can be reduced significantly. Therefore any complex terrain calibration and changes in the wind direction can be avoided. However, close distance lidar measurements are affected by the presence of the wind turbine, due to its induction zone. In this work, the dynamic coupling between changes in the wind turbine operating point and the velocities inside the induction zone is studied. Reynolds-Averaged Navier-Stokes (RANS) simulations are used to investigate this interaction. Thereafter, system identification is used to fit first order dynamic models to the simulation results. The parameters of the model are given for the turbine induction zone. These results possibly reduce the uncertainty in lidar measurements, arising from wind turbine blockage.

1. Introduction

Lidar sensors prove to be very helpful in the wind energy industry for different reasons. They can be used for yaw corrections [3], pitch control [12] and power and loads verifications [2]. Nevertheless, there are different issues with lidar measurements. One of the issues is the difficulty of wind speed measurements very close to the rotor disc (e.g. less than one rotor diameter). Close range measurements are being used in order to minimize the uncertainty due to the terrain etc. on the wind field measurements. In this case the effect of the induction zone of the rotor is prominent in the measurements. In [14] the authors have used SOWFA [1] for Large Eddy Simulations (LES) of a wind turbine model in a wind field in order to investigate the effect of the induction zone on lidar measurements. The authors have compared the simulation measurements in terms of mean wind velocity and turbulence intensity in the steady state conditions. Another investigation of the induction zone effect is presented in [13] where the wind field in the induction zone of a Vestas V27 is investigated.

In this work we address the problem with close range measurements where the lidar measurements are close enough to be affected by the induction of the rotor. Specifically, we will investigate the dynamic effect of the induction zone on the lidar measurements. We will show that changes in the operating point of the turbine affects the wind speed in the induction zone. Moreover, we will find the appropriate dynamic model that represents this behavior. The



Content from this work may be used under the terms of the [Creative Commons Attribution 3.0 licence](#). Any further distribution of this work must maintain attribution to the author(s) and the title of the work, journal citation and DOI.

results of this work can be used to reduce the uncertainty in the wind speed measurements close to the rotor disc.

2. Simulation setup

2.1. Numerical setup

The simulations are performed solving the incompressible transient Reynolds Averaged Navier-Stokes (RANS) equations with uniform non-turbulent inflow, at a Reynolds number of 1.0×10^8 with respect to the rotor radius (R). The finite volume code EllipSys3D solves the RANS equations over a discretized block-structured domain [15, 8, 9] with collocated variables. Solving convective terms using the QUICK scheme [4] and the SIMPLE method [10] for the pressure-linked terms of the Navier-Stokes equations. A modified Rhie-Chow algorithm [11, 16] avoids decoupling velocity and pressure in the presence of discrete body forces originating from an actuator disc (AD). The effect of turbulence on the mean flow is accounted for using Menter's $k-\omega$ shear-stress transport turbulence model [6]. The turbine rotor is represented by an actuator disc. The loading on the rotor is uniform and only acting normal to the disc. The simulations are converged at an initial thrust coefficient C_{T_i} before at a specific point in time t_0 a change ΔC_T is initiated. The C_T of the rotor at a time t is given by:

$$C_T(t) = \begin{cases} C_{T_i} & \text{for } t \leq t_0 \\ C_{T_i} + \Delta C_T \left(1 - e^{-\frac{t-t_0}{\tau}}\right) & \text{for } t > t_0 \end{cases} \quad (1)$$

where τ determines the speed with which the change is applied. The time step Δt had its upper limit at 0.04 set by the CFL number. Furthermore the ratio of the maximal gradient of $C_T(t)$ to Δt was kept constant in-between the simulations:

$$\frac{\max(dC_T/dt)}{\Delta t} = \frac{\Delta C_T/\tau}{\Delta t} = \text{constant} \quad (2)$$

2.2. Turbine model

The turbine rotor was represented by an actuator disc. The loading on the rotor was uniform and only acting normal to the disc. The normal force thus acting over a sectional area ΔA of the actuator disc is:

$$F_N = \frac{1}{2} \rho_\infty V_\infty^2 C_T \Delta A \quad (3)$$

Only the thrust coefficient C_T was changed between simulations. Note that approximating the influence of a rotor with only normal forces corresponds to the ideal case where the tip speed ratio tends to infinity.

2.3. Numerical domain

A box domain with side lengths of 25 radii (R) minimises the impact of domain blockage ($\pi/25^2 = 0.5\%$). It contains a finely meshed box that surrounds the actuator disc located at its center as shown in figure 1. The rotor radius is discretized with 33 grid points giving an inner mesh spacing, which previously yielded sufficiently accurate results [7]. From the fine mesh the grid grows hyperbolically outwards. The frontal and side faces of the domain are set as Dirichlet boundaries, whereas and Neumann boundary condition is applied to the rear.

3. Modeling of the Dynamics

In this work, the dynamic effect of the rotor on the upstream induced velocities is modelled via a transfer function. The transfer function describes how the induced velocity respond to a step change in the rotor loading. The transfer function was found to be well represented by the

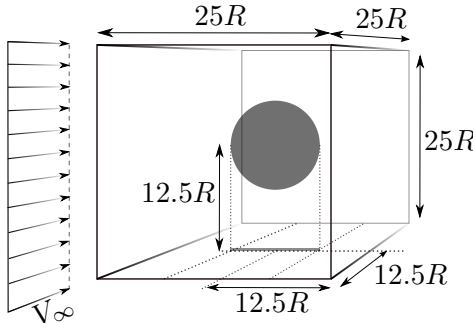


Figure 1: The numerical domain containing the actuator disc with uniform inflow. All dimensions are given in turbine radii.

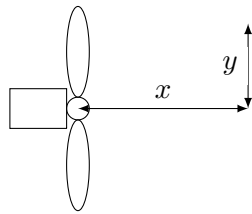


Figure 2: Probe points relative to the wind turbine, the wind turbine is seen from the top

following first order model:

$$H(s) = \frac{k(x, y)}{T(x, y)s + 1} \quad (4)$$

The two parameters to be identified are the gain of the system $k(x, y)$ and the time constant $T(x, y)$. These parameters are functions of space with the spatial coordinates x and y defined as shown in Figure 2. In order to illustrate the effect a change in the gain and time constant have on the transfer function, Figure 3 compares the response of the function with the following parameters:

$$H_1(s) = \frac{-0.1347}{1.4610s + 1} \quad (5)$$

$$H_2(s) = \frac{-0.0796}{1.4610s + 1} \quad (6)$$

$$H_3(s) = \frac{-0.1347}{1.8957s + 1} \quad (7)$$

H_1 and H_2 have the same time constant, but different gains. As it is seen in figure 3 they converge towards their respective steady state values with the same rate. However, the steady state values are different due to the different gains. H_1 and H_3 on the other hand converge to the same steady state value with different rates. This is because they have the same gain, but different time constants.

4. Results

System identification [5] is used to find an appropriate model that fits the dynamic changes in the wind speed at the probe point (x, y) , as the thrust coefficient changes. Figure 4 includes a sample response used for the system identification and the output of the identified model. This figure shows the changes in the wind speed at $(x, y) = (0.5R, 0)$ as a response to changes in the C_T for $\Delta C_T = 0.8$. The changes are shown as $\Delta V(t) = V(t) - V_0$, in which $V(t)$ is the

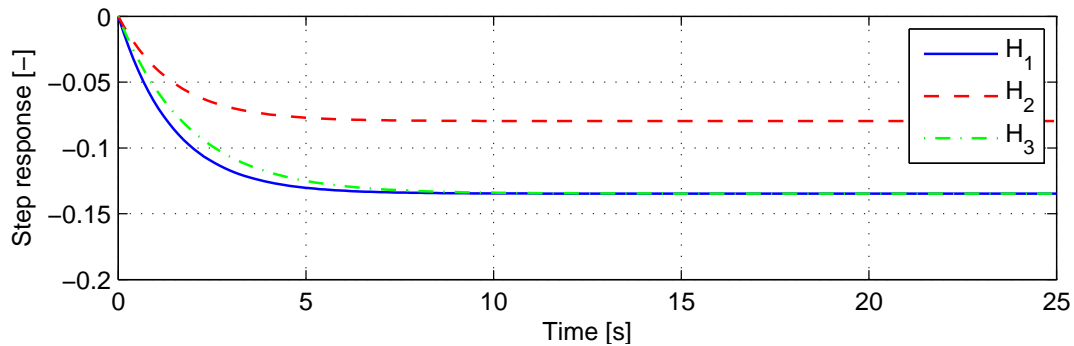


Figure 3: Step response comparison of three systems with different gains and time constant

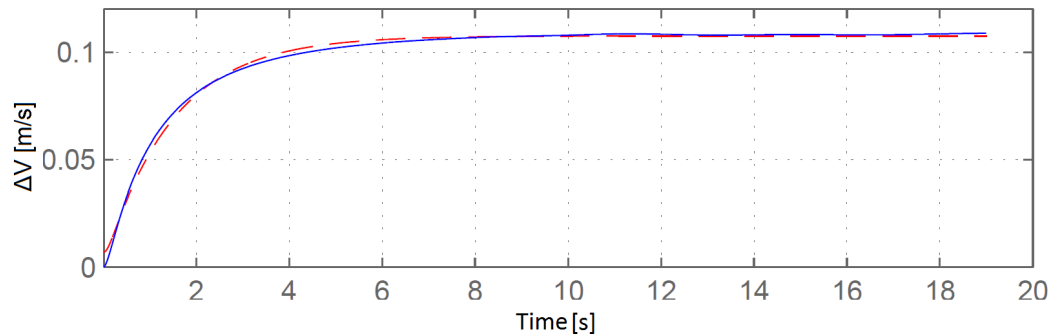


Figure 4: Changes in the wind speed as a result of changes in the C_T value in time, solid-blue is the predictions from CFD and red-dashed is the identified system

wind speed as a function of time and V_0 is the initial wind speed. System identification [5] is used to find an appropriate model that fits the dynamic changes in the wind speed at the probe point (x, y) , as the thrust coefficient changes. Figure 4 includes a sample response used for the system identification and the output of the identified model. This figure shows the changes in the wind speed at $(x, y) = (0.5R, 0)$ as a response to changes in the C_T for $\Delta C_T = 0.8$. The changes are shown as $\Delta V(t) = V(t) - V_0$, in which $V(t)$ shows the wind speed in time and $V(0)$ is the wind speed at initial time. The same identification procedure is used for the parameters of the transfer functions for the whole grid of $x-y$. The contour curve of the two parameters are given in figures 5 and 6. Figure 5 shows as x increases the amplitude of the gain of the transfer function decreases. This is natural, as when the probe point moves away from the rotor disc, the effect of the induction zone is reduced. Figure 6 shows that the dynamics, modeling changes in the CT, become slower as x increases. The figure shows that close to the turbine fast changes in the C_T have a prominent effect on the wind speed. As the measurement point moves away from the turbine, the fast changes are filtered and only slow changes in the C_T value can be observed.

5. Conclusions

In this paper the dynamic effect of changes in the operating point of the wind turbine on the wind speed measurements using lidars is investigated. It is observed that changes in the turbine operating point affect the upstream wind speed, and that the effect occurs dynamically. First order systems are used to capture this interaction. For each probe point or lidar measurement point upstream the wind turbine a model of the dynamic effect is identified and parameters of

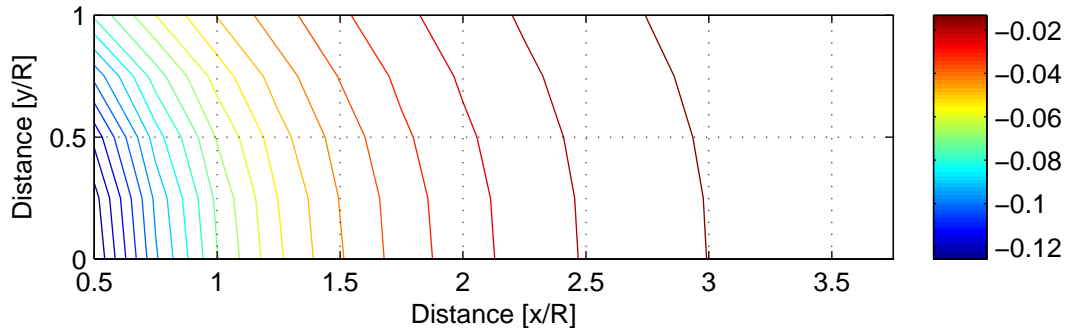


Figure 5: Gain of the transfer function $k(x, y)$

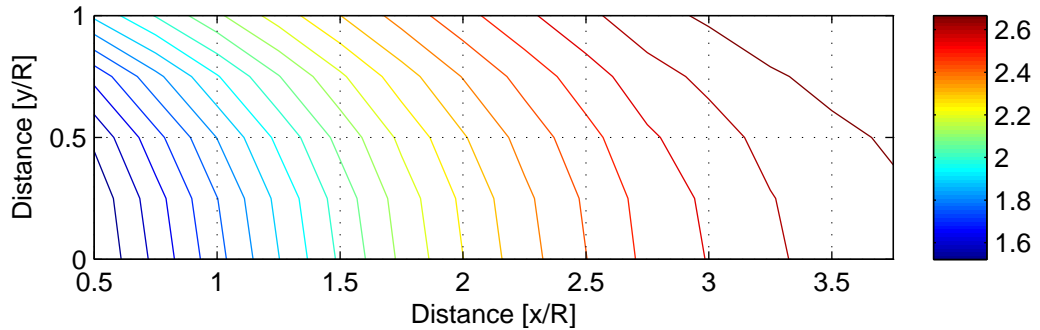


Figure 6: Time constant of the transfer function $T(x, y)$

the model determined. The results can be used to correct for the dynamic effect of the induction zone on the wind speed measurements. Furthermore, it allows to improve the estimation of the free stream wind speed by lidar measurements close to the rotor disc.

References

- [1] M. Churchfield and S. Lee. NWTC information portal (SOWFA), 2012.
- [2] N. K. Dimitrov and B. S. Lazarov. Reducing wind turbine load simulation uncertainties by means of a constrained gaussian turbulence field. *Proceedings of the 12th International Conference on Applications of Statistics and Probability in Civil Engineering (ICASP12)*, pages –, 2015.
- [3] P. A. Fleming, A. K. Scholbrock, A. Jehu, S. Davoust, E. Osler, A. D. Wright, and A. Clifton. Field-test results using a nacelle-mounted lidar for improving wind turbine power capture by reducing yaw misalignment. *Journal of Physics: Conference Series*, 524(1), 2014.
- [4] B. Leonard. A stable and accurate convective modelling procedure based on quadratic upstream interpolation. *Computer Methods in Applied Mechanics and Engineering*, 1979.
- [5] L. Ljung. *System identification / Theory for the user*. Prentice Hall, Upper Saddle River, N.J., 1999.
- [6] F. R. Menter. Zonal two equation $k - \omega$ turbulence models for aerodynamic flows. *AIAA Journal*, 1993.
- [7] A. Meyer Forsting and N. Troldborg. The effect of blockage on power production for laterally aligned wind turbines. *Journal of Physics: Conference Series (Online)*, 625, 2015.
- [8] J. Michelsen. Basis3D - a platform for development of multiblock PDE solvers. Technical report, Dept. of Fluid Mechanics, Technical University of Denmark, DTU, 1994.
- [9] J. Michelsen. Block structured multigrid solution of 2D and 3D elliptic PDE's. Technical report, Dept. of Fluid Mechanics, Technical University of Denmark, DTU, 1994.
- [10] S. Patankar and D. Spalding. A calculation procedure for heat, mass and momentum transfer in three-dimensional parabolic flows. *International Journal of Heat and Mass Transfer*, 1972.
- [11] P.-E. Réthoré and N. Sørensen. A discrete force allocation algorithm for modelling wind turbines in computational fluid dynamics. *Wind Energy*, 2012.
- [12] D. Schlipf and M. Kühn. Prospects of a collective pitch control by means of predictive disturbance

compensation assisted by wind speed measurements. In *Proceedings of the German Wind Energy Conference, DEWEK*, 2008.

- [13] E. Simley, N. Angelou, T. K. Mikkelsen, M. Sjöholm, J. Mann, and L. Y. Pao. Characterization of wind velocities in the upstream induction zone of a wind turbine using scanning continuous-wave lidars. *Journal of Renewable and Sustainable Energy, J Renew Sustain Ener, J. Renew. Sustain. Energy*, 8(1), 2016.
- [14] E. Simley, L. Y. Pao, P. Gebraad, and M. Churchfield. Investigation of the impact of the upstream induction zone on lidar measurement accuracy for wind turbine control applications using large-eddy simulation. *Journal of Physics. Conference Series*, 524(1), 2014.
- [15] N. Sørensen. *General purpose flow solver applied to flow over hills*. PhD thesis, Risø National Laboratory, 1995.
- [16] N. Troldborg, N. Sørensen, P.-E. Réthoré, and M. van der Laan. A consistent method for finite volume discretization of body forces on collocated grids applied to flow through an actuator disk. *Computers & Fluids*, 2015.